CrossMark

The Primary Proton Spectrum of the Hadronic PeVatron Candidate HAWC J1825-134

Timur Dzhatdoev[1,2,3] ⓘ, Egor Podlesnyi[1,2,4] ⓘ, and Igor Vaiman[1,2,4] ⓘ

[1] Federal State Budget Educational Institution of Higher Education, M.V. Lomonosov Moscow State University, Skobeltsyn Institute of Nuclear Physics (SINP MSU), 1(2), Leninskie gory, GSP-1, 119991 Moscow, Russia; timur1606@gmail.com, podlesnyi.ei14@physics.msu.ru
[2] Institute for Nuclear Research of the Russian Academy of Sciences, 60th October Anniversary Prospect 7a, Moscow 117312, Russia
[3] Institute for Cosmic Ray Research, University of Tokyo, 5-1-5 Kashiwanoha, Kashiwa, Japan
[4] Federal State Budget Educational Institution of Higher Education, M.V. Lomonosov Moscow State University, Department of Physics, 1(2), Leninskie gory, GSP-1, 119991 Moscow, Russia

Abstract

The γ-ray spectrum of the source HAWC J1825-134 measured with the High Altitude Water Cherenkov (HAWC) observatory extends beyond 200 TeV without any evidence for a steepening or cutoff. There are some indications that the γ-rays detected with HAWC were produced by cosmic-ray protons or nuclei colliding with the ambient gas. Assuming primary protons, we inquire which shape of the primary proton spectrum is compatible with the HAWC measurements. We find that the primary proton spectrum with the power-law shape of $\gamma_p = 2.2$ and the cutoff energy $E_{c-p} > 500$ TeV describes the data well. However, much harder spectra with γ_p down to 1.3 and E_{c-p} as low as 200 TeV also do not contradict the HAWC measurements. The former option might be realized if the accelerator is inside or very near to the γ-ray production zone. The latter option is viable for the case of a cosmic-ray source that effectively confines low-energy ($E_p < 10$ TeV) accelerated protons. Using publicly available data of the Fermi-LAT space γ-ray telescope, we derive upper limits on the intensity of the HAWC J1825-134 source in the 1 GeV–1 TeV energy range. We show that the account of these upper limits drastically changes the interpretation: only hard ($\gamma_p < 1.7$) spectra describe the combined HAWC and Fermi-LAT data sets well.

Unified Astronomy Thesaurus concepts: Gamma-ray astronomy (628); Gamma-ray sources (633); Gamma-rays (637); Gamma-ray observatories (632); Galactic cosmic rays (567); High energy astrophysics (739)

1. Introduction

Cosmic rays up to the so-called "knee"—a steepening in the all-nuclei spectrum measured at Earth (Kulikov & Khristiansen 1959; Aglietta et al. 2004; Antoni et al. 2005)—are widely believed to have a Galactic origin. The acceleration and propagation of cosmic-ray (CR) protons and nuclei colliding with the ambient gas are accompanied by the production of γ-rays (Stecker 1970, 1973; Black & Fazio 1973; Caraveo et al. 1980; Ackermann et al. 2012; Albert et al. 2021a). Therefore, Galactic hadronic PeVatrons—the objects accelerating protons up to the knee—could be searched for and studied with γ-astronomical methods.

So far, the search for these objects was not very successful. Indeed, γ-ray spectra of supernova remnants reveal a high-energy cutoff (Ahnen et al. 2017; Abdalla et al. 2018). The spectrum of the Cygnus Cocoon complex containing star-forming regions that could accelerate cosmic rays (Montmerle 1979; Cesarsky & Montmerle 1983; Bykov 2014; Bykov et al. 2018; Aharonian et al. 2019) also reveals a steepening at 10 TeV (Abeysekara et al. 2021).[5] The superhigh energy ($E > 100$ TeV) emission from pulsar wind nebulae (Amenomori et al. 2019; Abeysekara et al. 2020) is well explained with the leptonic mechanism (Khangulyan et al. 2019; Breuhaus et al. 2021). PeV protons could be accelerated near the Galactic Center (Abramowski

et al. 2016), but it is not clear whether these protons could make a substantial contribution to the CR flux observed at Earth.

Very recently, the High Altitude Water Cherenkov (HAWC) collaboration reported a measurement of the γ-ray spectrum of the source HAWC J1825-134 up to the energy of 300 TeV (Albert et al. 2021b, hereafter A21). The spectrum does not reveal any steepening or cutoff. A21 argue that the observed γ-rays were produced by the hadronic mechanism.

In the present paper we put constraints on the parameters of the primary CR spectrum, taking the HAWC results at face value and assuming that all γ-rays detected by HAWC from this source were produced by primary protons.[6] In Section 2, we dissect the region of the sky containing HAWC J1825-134. In Section 3, we set upper limits on the spectral energy distribution (SED = $E_\gamma^2 dN_\gamma/dE_\gamma$) of the source in the energy range of 1 GeV–1 TeV using publicly available Fermi Large Area Telescope (Fermi-LAT) data (Atwood et al. 2009).

In Section 4, we provide a few examples of a plausible primary proton spectrum that could explain the HAWC data reasonably well. We perform a scan on the parameters of the primary proton spectrum in Section 5. Finally, we discuss the obtained results in Section 6 and conclude in Section 7.

2. The HAWC J1825-134 Source and Its Surroundings

The HAWC J1825-134 source is situated in a crowded region of the γ-ray sky (see Figure 1). In A21, the HAWC collaboration presents a new analysis of this region, identifying

---

[5] However, the authors argue that the time-averaged CR spectrum in some time-dependent models could be harder than in stationary models.

[6] More precisely, by secondary particles produced by primary protons.
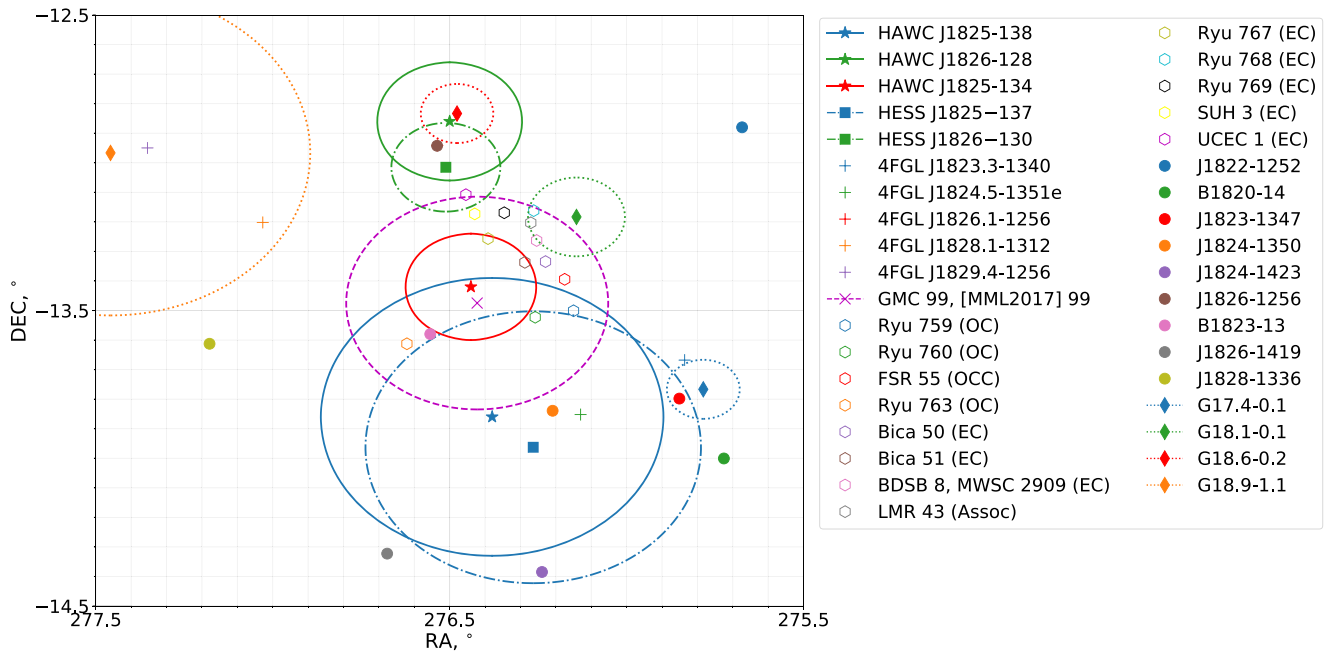
Figure 1. A view of the HAWC J1825-134 region (see the text for more details).

three bright TeV sources[7] shown in Figure 1 as stars: HAWC J1825-134 itself, as well as HAWC J1826-128 and HAWC J1825-138. The H.E.S.S. imaging Cherenkov telescope array (IACT) detected the likely counterparts of HAWC J1826-128 and HAWC J1825-138—the sources HESS J1826-130 (Abdalla et al. 2020) and HESS J1825-137 (Abdalla et al. 2019), respectively (denoted by squares in the figure). The extensions for HAWC sources are shown as solid circles,[8] and for H.E.S.S. sources as dotted–dashed circles. Statistical and systematic uncertainties of H.E.S.S. and HAWC source position measurements are not shown. The positions of Fermi-LAT sources from the 4FGL catalog (Abdollahi et al. 2020) (without extensions and position measurement uncertainties) are shown in Figure 1 as plus signs.

The giant molecular cloud GMC 99 (an alternative name is [MML2017] 99) (Miville-Deschênes et al. 2016) with the angular radius of $0°.36$ is shown in Figure 1 as a dashed magenta circle; its center is denoted as a magenta cross. Hollow hexagons denote objects from the multiband catalog of star clusters, associations, and candidates according to Bica et al. (2018); angular sizes are not shown and only objects within an $0°.4$ square with the center at $(276°.5, -13°.5)$ are shown. Filled circles denote pulsars from the ATNF catalog of Manchester et al. (2005a, 2005b); diamonds denote SNRs with their extensions shown as dotted circles according to Green (2019a, 2019b). Object names are shown in the legend. For the objects from the catalog of Bica et al. (2018) the object type is shown in parentheses after its name(s): OC for open cluster, OCC for open cluster candidate, EC for embedded cluster, and Assoc for star association.

Star-forming regions are among the possible sources of Galactic cosmic rays up to the knee. In particular, primary protons producing γ-rays responsible for the HAWC J1825-

134 source could have been accelerated in the embedded young star cluster BDSB 8 (MWSC2909) as proposed in A21 (the distance $D \approx 4.4$ kpc from the Sun; Kharchenko et al. 2016). A tentative target for protons producing γ-ray emission of the HAWC J1825-134 source is the core of GMC 99 ($D \approx 3.9$ kpc; Miville-Deschênes et al. 2016). For Bica 51 $D \approx 1.4$ kpc (Kharchenko et al. 2016), and for SUH 3 $D \approx 2.9$ kpc (Kurtz et al. 1994); therefore, these are unlikely sources of protons in HAWC J1825-134. For LMR 43, $D \approx 3.7 \pm 1.7$ kpc (Lee et al. 2012); for ECs Bica 50, Ryu 767, Ryu 768, Ryu 769, and UCEC 1 we could not find estimates of D. Therefore, we cannot exclude them from being possible sources of very high-energy protons for HAWC J1825-134.

3. Fermi-LAT Data Analysis

Remarkably, the HAWC J1825-134 source does not have any 4FGL counterparts. We use Fermi-LAT data[9] from 2008 August 4 to 2021 January 28 in the energy range from 1 GeV to 1 TeV. The region of interest (ROI) is a circle with the radius $R_{ROI} = 10°$ centered at the best-fit position of HAWC J1825-134 $(276°.44, -13°.42)$ reported in A21.

We performed a binned likelihood analysis of this data set using *fermipy* (Wood et al. 2017) (version 0.17.4) and *fermitools*[10] (version 1.2.23) packages assuming a model of the ROI containing the sources from the 4FGL catalog (Abdollahi et al. 2020), the diffuse galactic background, the isotropic γ-ray background, and the model of the source in question as a point source with a simple power-law spectrum at the center of the ROI. Some details of this analysis are available in Appendix A.
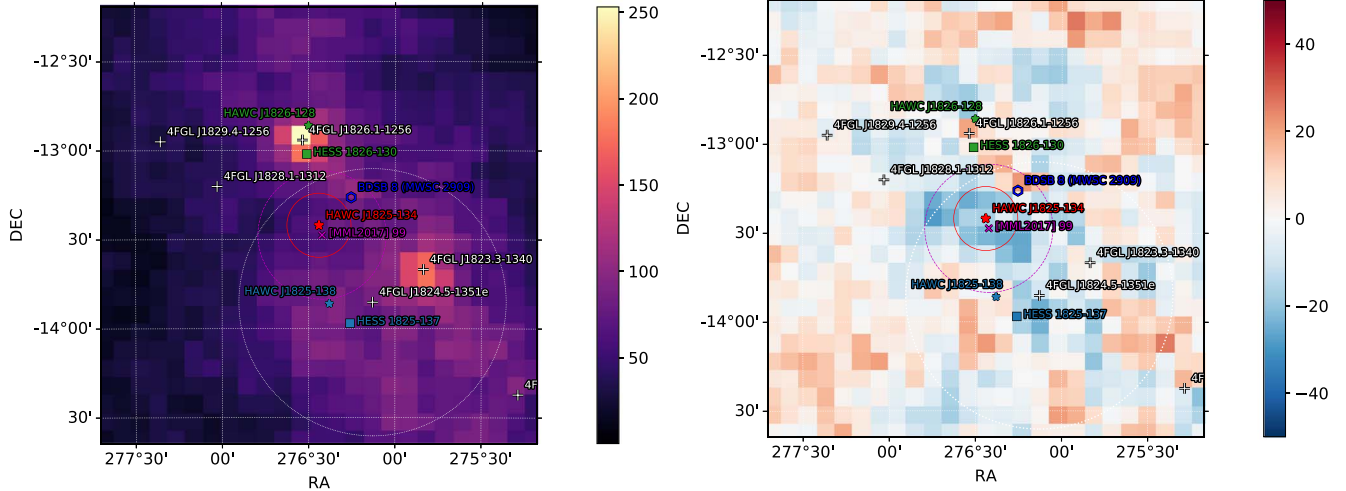
The test statistic (TS) corresponding to the hypothesis of the source HAWC J1825-134 being present in the model against the null hypothesis of the source being absent was calculated.

---

[7] Besides the Galactic diffuse emission.
[8] For HAWC J1825-138 and HAWC J1826-128 circles represent widths from Table 1 in A21, and for HAWC J1825-134 the circle represents the $0°.18$ upper limit on the extension of the source (95% confidence level).

[9] https://fermi.gsfc.nasa.gov/cgi-bin/ssc/LAT/LATDataQuery.cgi
[10] https://github.com/fermi-lat/Fermitools-conda

Figure 2. Fermi-LAT maps ($E \geqslant 10$ GeV) of the HAWC J1825-134 region. Left: Fermi-LAT count map. Right: Fermi-LAT excess map.

We obtained $TS \ll 1$, i.e., no significant signal from the source was observed.

A21 noted that there might be a systematic shift of about $0°.2$ in the HAWC J1825-134 source position. To ensure that this systematic error does not modify the negative result of our search, we also performed the source localization procedure using the `fermipy.GTAnalysis.localize` method searching for a better position of the source in question inside the $0°.5$ square with the center coinciding with the ROI center. This search yielded negative results.

Figure 2 shows the surroundings of HAWC J1825-134 as seen by Fermi-LAT for the energy $E \geqslant 10$ GeV:[11] the count map with the pixel size of $0°.1$ per pixel is shown on the left, and the excess count map (i.e., the map of the difference between the observed number of counts and the predicted number of counts of the fitted model in every pixel) with the same pixel size is shown on the right.

The position of HAWC J1825-134 is marked with a red star with a red solid circle representing the upper limit on its extension. The H.E.S.S. sources are shown as green and light blue squares, other HAWC sources as green and light blue stars, [MML2017] 99 as a magenta cross with the extension shown as a magenta dashed circle, EC BDSB 8 (MWSC 2909) as blue hollow hexagon, and Fermi-LAT sources as white plus signs.

The model describes the data reasonably well. Although there is some excess in some pixels near the pulsar 4FGL J1826.1-1256, this excess overshoots the model by only about 10% and occurs far from the position of HAWC J1825-134 reported in A21. Since the HAWC J1825-134 source $TS \ll 1$, it does not yield any predicted counts in the best-fit model. In the $0°.18$-vicinity of HAWC J1825-134 there is even a slight deficit of photon counts. The source in question is located inside the extension circle of the pulsar wind nebula (PWN) 4FGL J1824.5-1351e with the extension radius $0°.75$ (Abdollahi et al. 2020) shown in Figure 2 as a white dotted circle.

Comprehensive studies of this PWN associated with HESS J1825-137 were carried out by Araya et al. (2019) and Principe et al. (2020), and they did not find a source coincident with the position of HAWC J1825-134. Thus our negative result of the
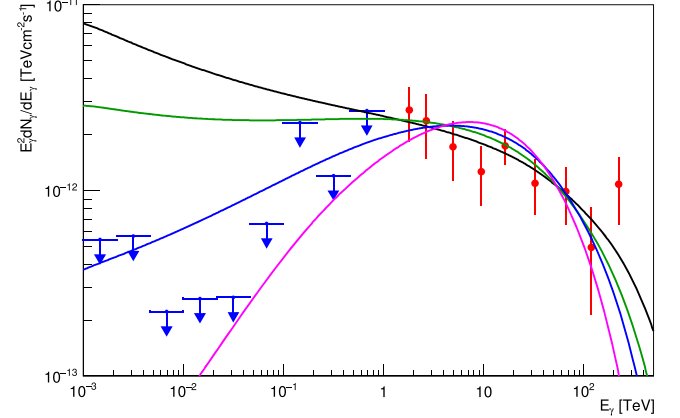
Figure 3. SED of HAWC J1825-134 measured with HAWC (red circles with statistical uncertainties) together with Fermi-LAT upper limits (blue arrows) as well as four model curves calculated for various proton spectrum parameters (see text for more details).

search for the γ-ray emission from HAWC J1825-134 is in agreement with the previous studies.

Finally, we obtained upper limits (95% confidence level) on the SED of HAWC J1825-134 using the `fermipy.GTAnalysis.sed` method allowing the source in question to have different spectral index values in different energy bins. These upper limits are shown in Figure 3 as blue arrows. In Appendix B we compare the upper limits on the SED of HAWC J1825-134 under the point-like source and extended source hypotheses.
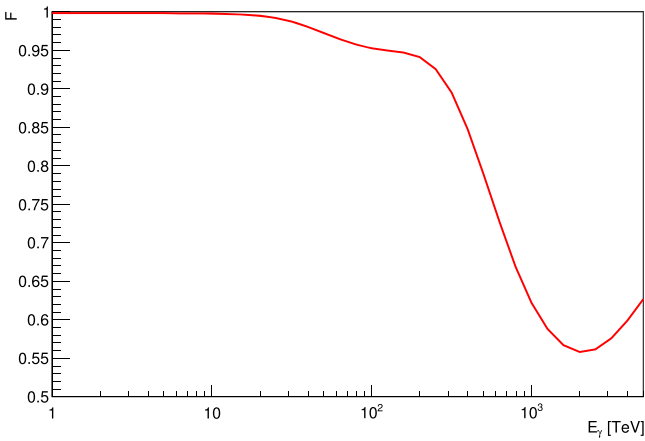
4. Examples of the Primary Proton Spectrum

In what follows we take the HAWC results concerning the analysis of the HAWC J1825-134 source at face value. The spectral energy distribution of HAWC J1825-134 according to A21 is shown in Figure 3 as red circles. Four model γ-ray SEDs are also shown in this figure, assuming a hadronuclear (more precisely, proton–proton) mechanism of γ-ray production on optically thin matter.[12]

---

[11] We show maps for $E \geqslant 10$ GeV since Fermi-LAT reaches the best angular resolution about $0°.1$ at energies $E \geqslant 10$ GeV allowing us to better discern different sources.

[12] That is, neglecting the contribution of cascade γ-rays to the observable γ-ray spectrum; given that the average gas column density from the region of HAWC J1825-134 is $N_H = 3 \times 10^{22}$ cm^{-2} (see A21), this assumption is justified.

Figure 4. γ-ray survival factor $F(E_\gamma) = e^{-\tau(E_\gamma)}$ vs. the γ-ray energy E_γ.

These SEDs were calculated using approximations of Kelner et al. (2006) under the assumption of the primary proton spectrum $\propto E^{-\gamma_p} \exp(-E_p/E_{p-c})$. The black curve corresponds to the case of $\gamma_p = 2.2$ and $E_{p-c} = 3$ PeV, green curve — $\gamma_p = 2.06$ and $E_{p-c} = 1$ PeV, blue curve — $\gamma_p = 1.8$ and $E_{p-c} = 500$ TeV, and magenta curve — $\gamma_p = 1.3$ and $E_{p-c} = 200$ TeV.

For simplicity, we neglect the bremsstrahlung of electrons produced together with γ-rays. The γ-ray absorption effect in the Galactic volume between the source and the observer was included according to Vernetto & Lipari (2016). The γ-ray survival factor $F(E_\gamma) = e^{-\tau(E_\gamma)}$ is shown in Figure 4 ($\tau(E_\gamma)$ is the optical depth).

Since the γ-ray absorption effect on the interstellar radiation field and the cosmic microwave background is modest ($\leqslant 22\%$ flux attenuation for $E_\gamma < 500$ TeV), our results do not change significantly if another model (e.g., Moskalenko et al. 2006) is chosen. We leave the intrinsic absorption effects (i.e., possible attenuation of the γ-ray flux inside the source) for future studies.

5. Scan over Parameters

We performed an exhaustive scan over the values of the primary proton spectrum parameters (γ_p, E_{p-c}) in the range $\gamma_p = 1$–3 and $E_{p-c} = 10^{14}$–10^{16} eV. For every set of the parameters, a model histogram of the observable SED was computed in the HAWC energy bins. After that, the optimal normalization of the model SED was determined that minimizes the value of the χ^2 form. The optimized χ^2 value was converted to a p-value and then to Z-value (statistical significance) according to the prescriptions of Zyla et al. (2020).

5.1. The Case of the Power-law Exponential Cutoff Primary Proton Spectrum

The resulting 100×100 matrix of the Z-value versus (γ_p, E_{p-c}) for the case of the primary proton spectrum $\propto E^{-\gamma_p} \exp(-E_p/E_{p-c})$ is shown in Figure 5 (left). All values of the Z-value below 1.0 are shown in Figure 5 (left) in the same color.

In particular, it turns out that the primary proton spectrum with parameters $\gamma_p = 2.2$ and $E_{p-c} = 3$ PeV describes the HAWC data well. However, some harder spectra with relatively low values of E_{p-c} (such as $\gamma_p = 2.06$ and $E_{p-c} = 1$ PeV; $\gamma_p = 1.8$ and $E_{p-c} = 500$ TeV; or even $\gamma_p = 1.3$ and $E_{p-c} = 200$ TeV) formally do not contradict the HAWC data.

In Figure 5 (right) we show the result of the same procedure, but accounting for the Fermi-LAT upper limits. The area contradicting these upper limits is shown in white. We conclude that the account of the Fermi-LAT upper limits drastically changes the interpretation, allowing to exclude soft ($\gamma_p > 1.8$) primary proton spectra for all considered values of E_{p-c}.

5.2. The Case of the Power-law Primary Proton Spectrum

It is worth considering a particular case of the primary proton power-law spectrum (i.e., the spectrum without a high-energy cutoff). Indeed, the spectrum of the Cygnus region measured with the LHAASO array (Cao et al. 2021) does not indicate a high-energy cutoff.

The dependence of the Z-value on the power-law index of the proton spectrum γ_p for this case is shown in Figure 6. The best fit of the HAWC data is achieved for $\gamma_p = 2.36$. In order to satisfy the Fermi-LAT upper limits, a low-energy break in the proton spectrum would be required. Indeed, if such a break is absent, the Fermi-LAT upper limits are overshot for $\gamma_p > 1.88$.

The assumption of the log-parabolic primary proton spectrum does not change our conclusions qualitatively. Finally, we note that the account of an additional γ-ray component which contributes mainly at relatively low energies (for instance, γ-rays from bremsstrahlung) would require even harder primary proton spectra, reinforcing our conclusions.

6. Discussion

6.1. The Acceleration Spectrum and the Effective γ-Ray Production Spectrum

It is widely believed that a typical Galactic hadronic PeVatron has a spectrum of protons with $\gamma_p = 2.0$–2.3 and $E_{p-c} = 1$–3 PeV. However, the γ-ray production zone is not necessarily spatially coincident with the particle acceleration zone. The primary proton spectrum may be significantly modified by propagation effects (Aharonian & Atoyan 1996) associated with escape from the accelerator (e.g., Moskalenko et al. 2008), diffusion from the accelerator to the γ-ray production zone, etc. Therefore, a hard "effective" spectrum of protons with $\gamma_p = 1.8$ or even $\gamma_p = 1.3$ could not be excluded a priori. We note that Bykov et al. (2018) predicted very hard spectra of accelerated particles at the energy significantly below the maximum acceleration energy; our results are consistent with this prediction.

6.2. Statistical Considerations

The results of this study could be somewhat influenced by several statistical effects, including (a) migration of events between the energy bins of the HAWC spectrum, and (b) a possible Eddington bias in the last energy bin. An account of the first effect is likely to result in an increase of the minimal value of E_{p-c} compatible with the HAWC data.

The Eddington bias (Eddington 1913) is a statistical effect that occurs when a population of sources is observed by an instrument of limited sensitivity, resulting in an overestimation of the flux of some of these sources. A discussion of this effect could be found in, e.g., Strotjohann et al. (2019). The sources with unusually high maximal γ-ray energy $E_{\gamma-\max}$ sometimes receive extra attention, even if the apparently high value of $E_{\gamma-\max}$ is partly due to statistical fluctuations. That said, this effect affects mainly the very last bin of the energy spectrum of HAWC J1825-134.
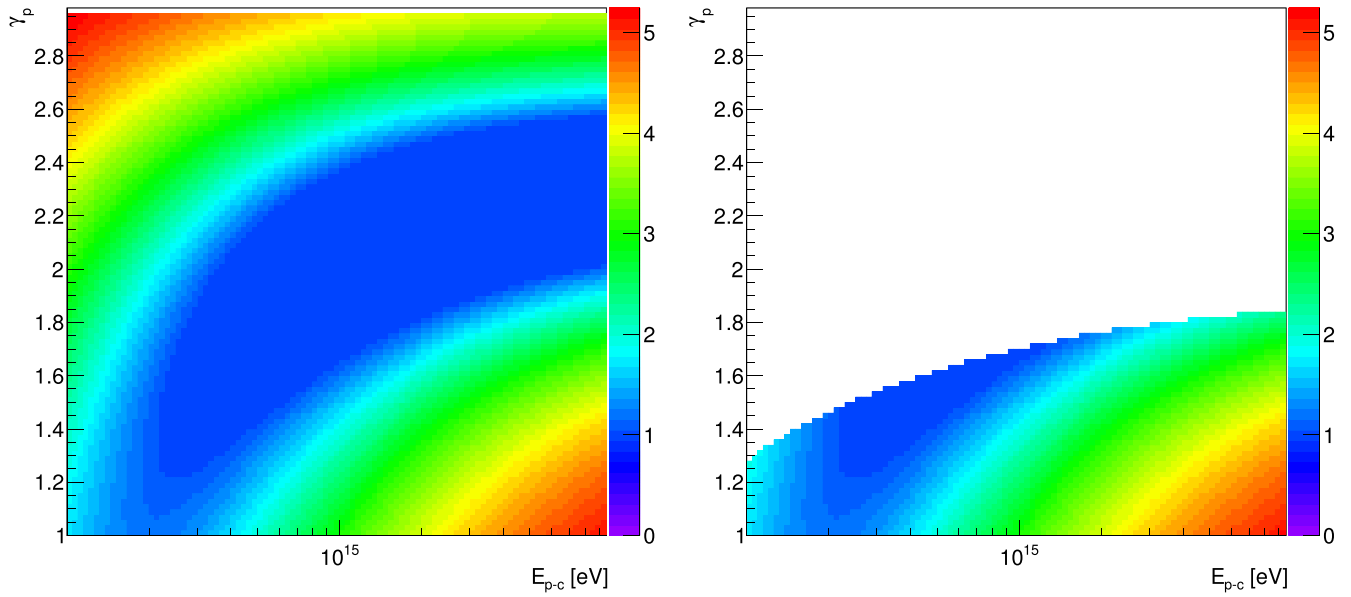
Figure 5. Exclusion significance (Z-value) vs. the primary proton spectrum parameters. Left: only HAWC data accounted for. Right: HAWC data and Fermi-LAT upper limits accounted for (the Fermi-LAT upper limits are overshot in the white region of the parameter area).
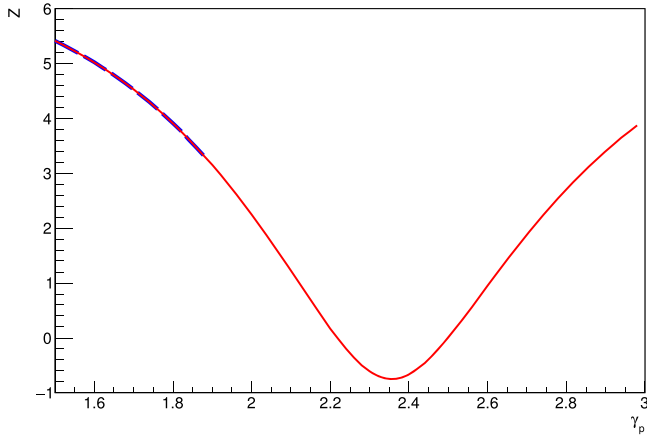
Figure 6. Exclusion significance (Z-value) vs. the power-law index of the proton spectrum. Red solid line: only HAWC data accounted for. Blue dashed line: HAWC data and Fermi-LAT upper limits accounted for.

The Eddington bias would lead to an overestimation of the observable flux at the last energy bin. Therefore, a correction for this statistical effect would decrease the minimal value of E_{p-c} compatible with the HAWC data. To some extent, these two effects partially compensate for each other.

6.3. Prospects of Neutrino Detection from HAWC J1825-134

HAWC J1825-134 is a promising Galactic neutrino source (Niro et al. 2021). Therefore, some hints about the nature of this source could potentially be obtained from astrophysical neutrino observations. We leave this study for future works.

7. Conclusions

The HAWC data alone do not allow one to exclude the hypothesis of $E_{p-c} < 1$ PeV for the HAWC J1825-134 source. Formally, a wide range of (γ_p, E_{p-c}) (down to $\gamma_p = 1.3$ and $E_{p-c} = 200$ TeV) do not contradict the spectrum of this source measured with HAWC. The account of the Fermi-LAT upper limits allowed us to exclude soft ($\gamma_p > 1.8$) primary proton

spectra for all considered values of E_{p-c}. Observations with the LHAASO (Cao et al. 2022) and CTA (Actis et al. 2011) detectors will be crucial in establishing the nature of this source.

Facilities: HAWC, Fermi-LAT.

Software: NumPy (Harris et al. 2020), *Astropy* (Price-Whelan et al. 2018), *Matplotlib* (Hunter 2007), *ROOT* (Brun & Rademakers 1997).

Appendix A
Fermi-LAT Data Analysis Details

In our Fermi-LAT data analysis of the 10° ROI centered at the position of HAWC J1825-134 we apply a cut on the zenith angle value $\theta_z \leqslant 90°$ in order to remove contamination from the Earth's limb. We used the `P8R3_SOURCE_V2` instrument response function (`evclass = 128`) with events of both front and back type of the γ-ray conversion location (`evtype = 3`).[13] To describe the observed γ-ray emission we constructed a model containing all sources from the 4th Fermi-LAT source catalog 4FGL (Abdollahi et al. 2020) located within 15° from the center of the ROI, the model of the diffuse galactic background `gll_iem_v07`, the model of the isotropic γ-ray background `iso_P8R3_SOURCE_V2_v1`,[14] and the model

---

[13] https://fermi.gsfc.nasa.gov/ssc/data/analysis/documentation/Cicerone/Cicerone_LAT_IRFs/IRF_overview.html
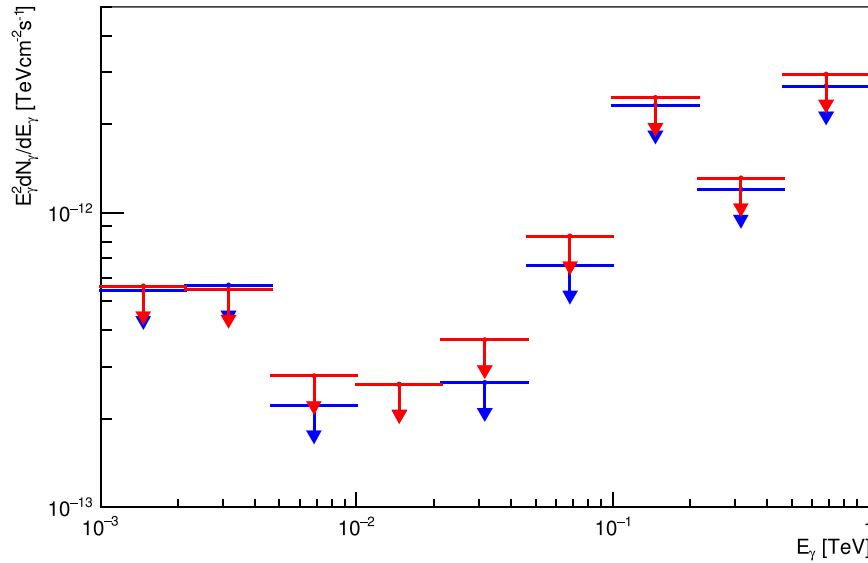[14] https://fermi.gsfc.nasa.gov/ssc/data/access/lat/BackgroundModels.html

of the source in question as a point source with a simple power-law spectrum[15] at the center of the ROI. Spectral shapes and normalization of diffuse backgrounds and the source in question were left free, normalization of other sources within $5°$ from the center of the ROI was also left free, but their spectral shapes were fixed; both normalization and spectral shapes of other sources outside $5°$ from the ROI center were fixed to their catalog values. In our analysis the energy dispersion was taken into account for all sources except for the diffuse galactic background and the isotropic γ-ray background. Using this ROI model we performed the maximization of the binned likelihood function in the considered energy range using the `fermipy.GTAnalysis.optimize` and `fermipy.GTAnalysis.fit` methods. The results of the likelihood analysis are discussed in Section 3.

Appendix B
Analysis with the Extended Source Model

We also performed a Fermi-LAT data analysis with the extended source model. All parameters of the constructed model were the same as described in Appendix A, except for the spatial model of HAWC J1825-134, which has been changed from the point source to the extended symmetric 2D radial Gaussian source with the 95% containment radius of $0°.18$, which is equal to the 95% confidence level upper limit on the extension of HAWC J1825-134 derived in A21. The obtained upper limits on the SED for both spatial models of HAWC J1825-134 are shown in Figure 7. We note that the slight difference between the two versions of the SED upper limits does not modify our conclusions.

Figure 7. Comparison of the upper limits on the SED of HAWC J1825-134 for the point source (blue arrows) and extended source (red arrows) spatial models.

15 https://fermi.gsfc.nasa.gov/ssc/data/analysis/scitools/xml:model_defs.html

ORCID iDs

Timur Dzhatdoev ● https://orcid.org/0000-0002-7660-4236
Egor Podlesnyi ● https://orcid.org/0000-0003-3395-0419
Igor Vaiman ● https://orcid.org/0000-0002-8255-3631

References

Abdalla, H., Abramowski, A., Aharonian, F., et al. 2018, A&A, 612, A6
Abdalla, H., Adam, R., Aharonian, F., et al. 2020, A&A, 644, A112
Abdalla, H., Aharonian, F., Benkhali, F. A., et al. 2019, A&A, 621, A116
Abdollahi, S., Acero, F., Ackermann, M., et al. 2020, ApJS, 247, 33
Abeysekara, A., Albert, A., Alfaro, R., et al. 2020, PhRvL, 124, 021102
Abeysekara, A. U., Albert, A., Alfaro, R., et al. 2021, NatAs, 5, 465
Abramowski, A., Aharonian, F., Benkhali, F. A., et al. 2016, Natur, 531, 476
Ackermann, M., Ajello, M., Allafort, A., et al. 2012, ApJ, 755, 22
Actis, M., Agnetta, G., Aharonian, F., et al. 2011, ExA, 32, 193
Aglietta, M., Alessandro, B., Antonioli, P., et al. 2004, APh, 21, 583
Aharonian, F., Yang, R., & de Oña Wilhelmi, E. 2019, NatAs, 3, 561
Aharonian, F. A., & Atoyan, A. M. 1996, A&A, 309, 917
Ahnen, M. L., Ansoldi, S., Antonelli, L. A., et al. 2017, MNRAS, 472, 2956
Albert, A., Alfaro, R., Alvarez, C., et al. 2021a, ApJ, 914, 106
Albert, A., Alfaro, R., Alvarez, C., et al. 2021b, ApJL, 907, L30
Amenomori, M., Bao, Y., Bi, X., et al. 2019, PhRvL, 123, 051101
Antoni, T., Apel, W., Badea, A., et al. 2005, APh, 24, 1
Araya, M., Mitchell, A. M. W., & Parsons, R. D. 2019, MNRAS, 485, 1001
Atwood, W. B., Abdo, A. A., Ackermann, M., et al. 2009, ApJ, 697, 1071
Bica, E., Pavani, D. B., Bonatto, C. J., & Lima, E. F. 2018, AJ, 157, 12
Black, J. H., & Fazio, G. G. 1973, ApJ, 185, L7
Breuhaus, M., Hahn, J., Romoli, C., et al. 2021, ApJL, 908, L49
Brun, R., & Rademakers, F. 1997, NIM A, 389, 81
Bykov, A., Ellison, D., Gladilin, P., & Osipov, S. 2018, AdSpR, 62, 2764
Bykov, A. M. 2014, A&ARv, 22, 77
Cao, Z., Aharonian, F. A., An, Q., et al. 2021, Natur, 594, 33
Cao, Z., della Volpe, D., Liu, S., et al. 2022, ChPhC, 46, 035001
Caraveo, P. A., Bennett, K., Bignami, G. F., et al. 1980, A&A, 91, L3
Cesarsky, C. J., & Montmerle, T. 1983, SSRv, 36, 173
Eddington, A. S. 1913, MNRAS, 73, 359
Green, D. A. 2019a, JApA, 40, 36
Green, D. A. 2019b, A Catalogue of Galactic Supernova Remnants, http://www.mrao.cam.ac.uk/surveys/snrs/
Harris, C. R., Millman, K. J., van der Walt, S. J., et al. 2020, Natur, 585, 357
Hunter, J. D. 2007, CSE, 9, 90
Kelner, S. R., Aharonian, F. A., & Bugayov, V. V. 2006, PhRvD, 74, 034018
Khangulyan, D., Arakawa, M., & Aharonian, F. 2019, MNRAS, 491, 3217
Kharchenko, N. V., Piskunov, A. E., Schilbach, E., Roeser, S., & Scholz, R.-D. 2016, A&A, 585, A101
Kulikov, G., & Khristiansen, G. 1959, JETP, 35, 441
Kurtz, S., Churchwell, E., & Wood, D. O. S. 1994, ApJS, 91, 659
Lee, E. J., Murray, N., & Rahman, M. 2012, ApJ, 752, 146
Manchester, R. N., Hobbs, G. B., Teoh, A., & Hobbs, M. 2005a, AJ, 129, 1993
Manchester, R. N., Hobbs, G. B., Teoh, A., & Hobbs, M. 2005b, ATNF Pulsar Catalogue, 1, 64
Miville-Deschênes, M.-A., Murray, N., & Lee, E. J. 2016, ApJ, 834, 57
Montmerle, T. 1979, ApJ, 231, 95
Moskalenko, I. V., Porter, T. A., Malkov, M. A., & Diamond, P. H. 2008, ICRC (Mérida), 2, 763
Moskalenko, I. V., Porter, T. A., & Strong, A. W. 2006, ApJ, 640, L155
Niro, V., Neronov, A., Fusco, L., Gabici, S., & Semikoz, D. 2021, PhRvD, 104, 023017
Price-Whelan, A. M., Sipőcz, B. M., Günther, H. M., et al. 2018, AJ, 156, 123
Principe, G., Mitchell, A. M. W., Caroff, S., et al. 2020, A&A, 640, A76
Stecker, F. W. 1970, Ap&SS, 6, 377
Stecker, F. W. 1973, ApJ, 185, 499
Strotjohann, N. L., Kowalski, M., & Franckowiak, A. 2019, A&A, 622, L9
Vernetto, S., & Lipari, P. 2016, PhRvD, 94, 063009
Wood, M., Caputo, R., Charles, E., et al. 2017, arXiv:1707.09551
Zyla, P., Barnett, R. M., Beringer, J., et al. 2020, PTEP, 2020, 083C01